IL NUOVO CIMENTO **43 C** (2020) 34
DOI 10.1393/ncc/i2020-20034-3

COLLOQUIA: IFAE 2019

# ATLAS searches for resonances decaying to boson pairs

M. LAVORGNA(1)(2)(*)

(1) *INFN, Sezione di Napoli - Napoli, Italy*
(2) *Dipartimento di Fisica, Università degli Studi di Napoli Federico II - Napoli, Italy*

received 8 June 2020

**Summary.** — Searches for heavy-mass resonances decaying into a couple of vectorial bosons, $WW$, $WZ$ or $ZZ$ using data from proton-proton collisions at a centre-of-mass energy of $\sqrt{s} = 13\,\text{TeV}$ at the Large Hadron Collider are presented. The searches are performed in the semileptonic and fully hadronic final states, in which one boson decays into leptons and the other one decays into hadrons, or both bosons decay hadronically. Semileptonic results refer to an integrated luminosity of 36.1 $\text{fb}^{-1}$ recorded with the ATLAS detector in 2015–2016 while the fully hadronic results correspond to the full Run-II statistics, 139 $\text{fb}^{-1}$. These results are interpreted within the context of Standard Model extensions with additional Higgs bosons, a heavy vector triplet or warped extra dimensions.

## 1. – Introduction

One of the main goal of the physics programme at the Large Hadron Collider (LHC) [1] is the search for new phenomena that may become visible in high-energy proton-proton (pp) collisions. Many models of physics beyond the Standard Model (SM) predict as possible signature for new physics the production of a heavy resonance with the subsequent decay into a final state consisting of a pair of vector bosons ($WW$, $WZ$, $ZZ$). These include extensions to the SM scalar sector as in the two-Higgs-doublet model (2HDM) [2] that predict new spin-0 resonances. In the Heavy Vector Triplet (HVT) [3] phenomenological Lagrangian model, a new heavy vector triplet ($W'$, $Z'$) is introduced with the new gauge bosons degenerate in mass. Warped extra dimensions Randall-Sundrum (RS) models predict spin-2 Kaluza-Klein (KK) excitations of the graviton, $G_{KK}$ [4] and spin-0 radions [5].

(*) E-mail: marco.lavorgna@na.infn.it

Searches in fully hadronic final states have been reported and the results refer to an integrated luminosity of 139 $\text{fb}^{-1}$ recorded with the ATLAS detector [6] in the 2015–2018 Run-II data period at $\sqrt{s} = 13\,\text{TeV}$ [7].

Searches in final states in which one boson decays into leptons and the other one decays into hadrons are also reported and the results refer to an integrated luminosity of 36.1 $\text{fb}^{-1}$ [8, 9].

Resonance production mechanisms through gluon-gluon fusion (ggF), Drell-Yan (DY) and vector-boson fusion (VBF) processes are considered, depending on the assumed model.

Heavy resonances would manifest themselves as resonant structures above the SM background in the invariant-mass distributions of the final state and in the $X \to ZV \to \nu\nu qq$ channel as broad enhancements in the transverse-mass distributions of the $\nu\nu qq$ final state.

## 2. – The ATLAS experiment at LHC

ATLAS is a multipurpose experiment with analyses varying from Standard Model precision measurements to search for evidence of new physics. The ATLAS detector at the Large Hadron Collider surrounds nearly the entire solid angle around the collision point. It has an approximately cylindrical geometry and the experimental apparatus consists of an inner tracking detector surrounded by electromagnetic and hadronic calorimeters and a muon spectrometer. The inner detector is placed within a 2T axial magnetic field provided by a superconducting solenoid. It consists of silicon pixel, silicon microstrip and transition radiation detectors that cover the pseudorapidity range $|\eta| < 2.5$. It allows precise reconstruction of charged-particle trajectories and measurement of their momenta.

Electromagnetic and hadronic calorimeter systems provide energy measurements with high granularity. The electromagnetic calorimeter is a liquid-argon (LAr) sampling calorimeter with lead absorbers and the hadronic calorimeter is a sampling calorimeter where the iron is used as absorber material and the scintillator as active material. They cover the central pseudorapidity range $|\eta| < 1.7$ and in the endcap and forward regions are both LAr calorimeters covering the $|\eta| < 4.9$ range.

The muon spectrometer constitutes the outer part of the ATLAS detector and allows to indentify muons from 3 GeV to 1 TeV, providing precision muon tracking and triggering. It includes three large superconducting air-core toroids and tracking drift chambers. The barrel region covers the $|\eta| < 1.0$ range, while endcaps $|\eta| < 2.7$.

Events are recorded in ATLAS if they satisfy a two-level trigger requirement [10] that reduces the event rate to approximately 1kHz for offline investigations.

## 3. – Jet reconstruction and signal classification

The final state of the diboson analyses is characterized by two vector bosons that could decay hadronically, so jets reconstruction is a main feature of these kinds of analyses. As the momentum of the boson increases, the quarks pair is increasingly boosted, so if the resonance mass is significantly higher than the $V$ boson mass, the $qq$ pair from the $V$ boson decay can be collimated. In this case hadrons from the two quarks overlap in the detector and are more efficiently reconstructed as a single large-$R$ jet.

In the semileptonic analyses a mass range from 300 to 5000 GeV is investigated, and two different reconstruction techniques for the $V \to qq$ decay are considered: resolved and merged. The resolved reconstruction attempts to identify two separate small-radius jets of hadrons from the $V$ decay, while the merged reconstruction identifies the $V \to qq$ decay as a single large-$R$ jet, using jet substructure techniques.

In the fully hadronic analysis the mass range investigated starts from 1300 GeV, so only the merged regime is considered.

Jets must be consistent with the fact that they originate from hadronic decays of $W$ or $Z$ bosons. In the merged regime, discrimination against background jets is obtained by defining a mass window around the $W/Z$ mass and by cutting on the variable $D_2$. The variable $D_2$ is defined as a ratio of two-point to three-point energy correlation functions that are based on the energies and pairwise angular distances between the jet's constituents [11].

In the semileptonic final states different resonance production mechanisms are taken into account depending also on the assumed signal model: gluon-gluon fusion (ggF), Drell-Yan (DY) and vector-boson fusion (VBF) processes are considered. Although VBF events have lower cross sections with respect to the other production mechanisms, they have more information since in addition to the presence of a pair of vector bosons from the resonance decay, two additional jets are expected in the forward region of the detector. A good event classification can lead to an increase of signal sensitivity. The additional jets are characterized by a large separation in pseudorapidity and a large dijet invariant mass. A bidimensional selection in the $(m_{jj}, \Delta\eta_{jj})$ plane has been performed in order to categorize the events, optimizing the purity of the VBF signal while rejecting the background [8, 9].

## 4. – Fully hadronic analysis

The $X \to VV \to JJ$ analysis [7] is characterized by a fully hadronic final state. The $W$ and $Z$ bosons produced in the decay of high-mass resonances (TeV-scale) are highly boosted, therefore the final jets are reconstructed in ATLAS as a single large-$R$ jet. The hadronic decays of vector bosons have the largest branching ratio (67% for $W$ and 70% for $Z$ bosons) so this is the favoured diboson channel, but it suffers from background contamination from the production of multijet events. Multijet events constitute around 85% of the total background, while less relevant contributions come from Standard Model processes containing bosons, $V$+jets, diboson production $VV$, $t\bar{t}$ and single top production. In order to suppress the large contribution of the multijet processes, the characteristic jet substructure of $W/Z$ boson decays is used and requirements on the separation of the two jets are imposed.

The search for diboson resonances is performed by looking for narrow peaks above the smoothly falling $m_{JJ}$ distribution expected from the SM. The background to the search is estimated based on a fit to the observed $m_{JJ}$ spectrum in the signal region (fig. 1). This procedure is tested in dedicated CRs. Different signal regions are defined according to the type of the vector boson: $WW$, $ZZ$, $WZ$, $WW + ZZ$, $WW + WZ$.

Results for this analysis are obtained with the full Run-II statistics. To improve the sensitivity of this search, new techniques have been adopted since the publication of the results on the data collected in 2015–2016 (corresponding to the first 36 fb$^{-1}$ of data collected at $\sqrt{s} = 13$ TeV). A new type of object unifying tracking and calorimeter information, the Track-CaloCluster (TCC) [12], has been used as input to jet recon-

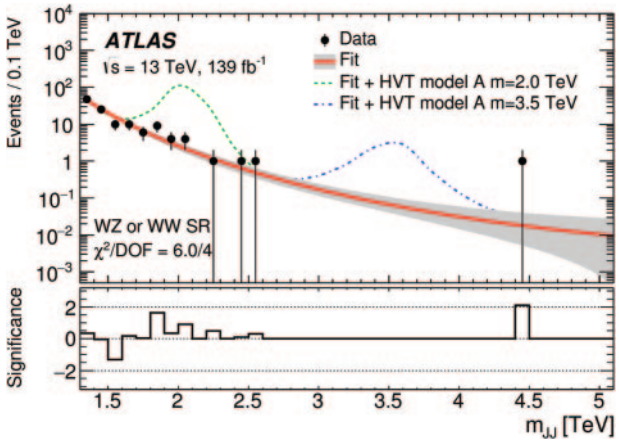


Fig. 1. – Background-only fits to the dijet mass $m_{jj}$ distributions in data in the combined $WW + WZ$ signal region. The shaded bands represent the uncertainty in the background expectation calculated from the maximum-likelihood function. The lower panel shows the significance, defined as the $z$-value as described in ref. [13]. Selected theoretical signal distributions are overlaid on top of the background [7].

struction in the full Run-II analysis. Moreover, improvements of the $W/Z$ tagger for the identification of the boosted jets have been performed.

More details about the fully hadronic analysis can be found in [7].

## 5. – Semileptonic analyses

The semileptonic analyses [8, 9] are characterized by two vector bosons, in which one decays hadronically while the other one leptonically, so we have three different final states according to the number of leptons in the final state: $X \to ZV \to \nu\nu qq$ (0 lepton channel), $X \to WV \to l\nu qq$ (1 lepton channel) and $X \to ZV \to llqq$ (2 lepton channel). These analyses perform a categorization of the events according to the resonance production mechanism and according to the resolved and merged regimes. Moreover, a categorization on the jets flavor and on the boson tagger working points for the identification of the boosted jets is used. Dedicated signal regions have been defined for each analysis to improve the sensitivity.

The main background processes for the $llqq$ analysis are the $Z$+jets, $t\bar{t}$, single top production and diboson production mainly from the SM $ZZ$ and $ZW$. For the $\nu\nu qq$ analysis the main backgrounds arise from $Z$+jets, $W$+jets and $t\bar{t}$ production. $W$+jets and $t\bar{t}$ production are also the main backgrounds for the $l\nu qq$ analysis. Dedicated control regions have been defined to estimate the different background components.

Figure 2 shows the final discriminant variables for the $H \to ZZ \to llqq/\nu\nu qq$ searches in the spin-0 signal hypothesis, and the final discriminant variable for the $Z' \to WW \to l\nu qq$ search in the spin-1 signal hypothesis.

More details about the semileptonic analyses can be found in [8, 9].

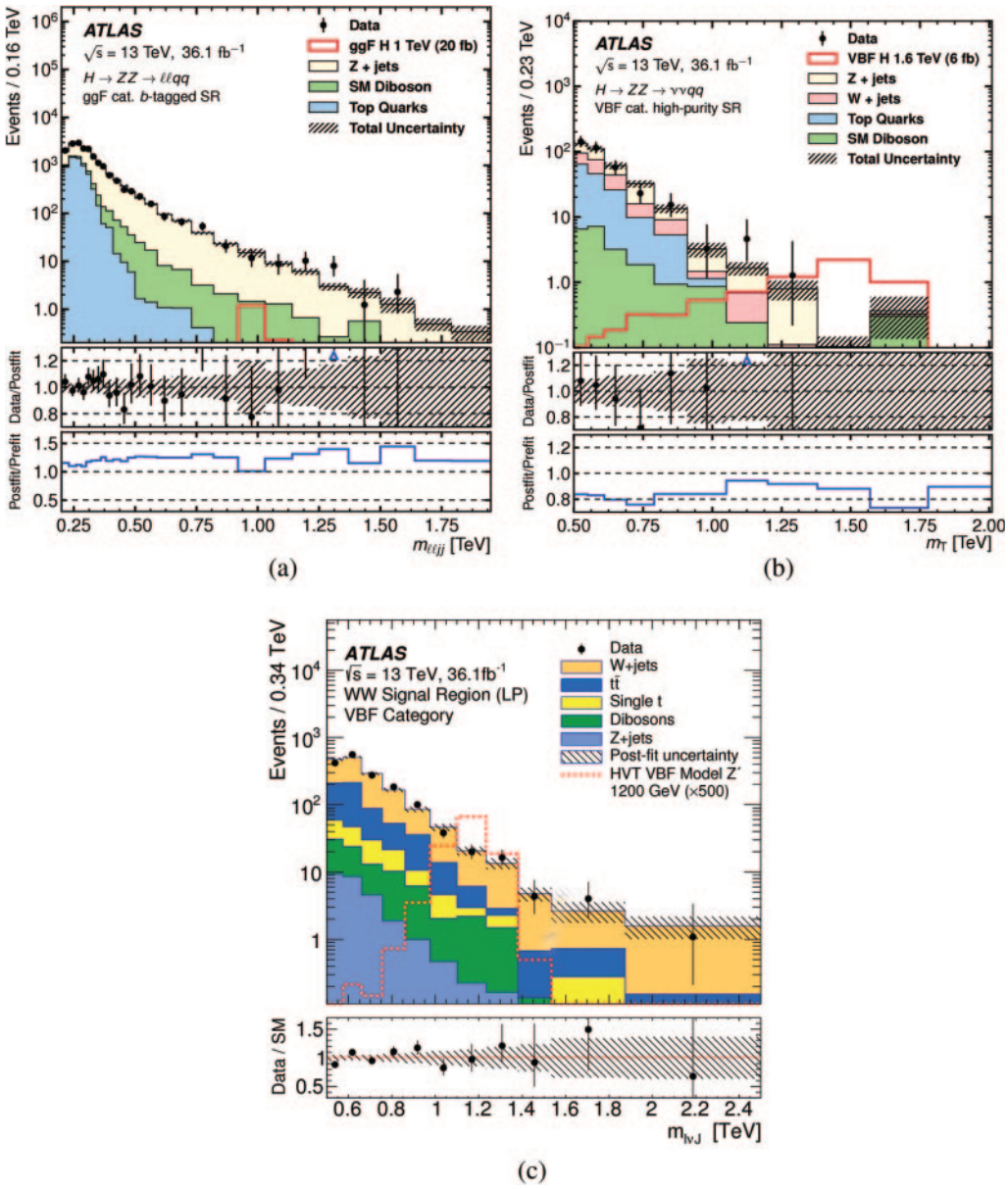


Fig. 2. – Comparisons of the observed data and expected background distributions of the final discriminants: (a) $m_{lljj}$ discriminant for ggF category for the $H \to ZZ \to llqq$ searches; (b) $m_T$ discriminant for VBF category for the $H \to ZZ \to \nu\nu qq$ search; (c) $m_{l\nu J}$ discriminant for VBF category for the $Z' \to WW \to l\nu qq$ search. Expected distribution from the ggF (VBF) production of a 1 TeV (1.6 TeV) Higgs boson in panels (a), (b) and VBF production of 1.2 TeV $Z'$ HVT boson in panel (c) are also shown [8, 9].

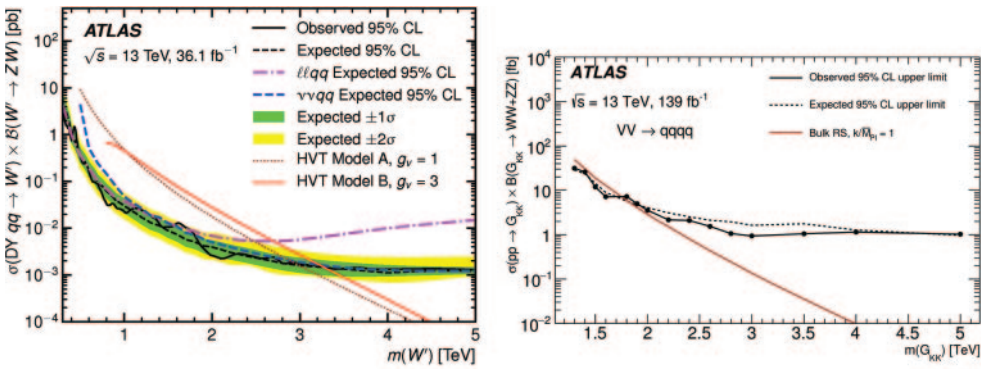


Fig. 3. – Observed (black solid curve) and expected (black dashed curve) 95% CL upper limits on: (a) $\sigma \times B(W' \to ZW)$ for the DY production of a $W'$ boson in the HVT model as a function of its mass, combining $llqq$ and $\nu\nu qq$ searches. Theoretical predictions are overlaid for HVT Model A and Model B. The green (inner) and yellow (outer) bands represent the $\pm 1\sigma$ and $\pm 2\sigma$ uncertainty in the expected limits [8]. (b) $\sigma \times B(G_{KK} \to WW + ZZ)$ for the DY production of a bulk RS graviton $G_{KK}$ as a function of its mass, in $qqqq$ search. Theoretical predictions are overlaid for the bulk RS model with $k/\overline{M}_{Pl} = 1$ [7].

## 6. – Results

Upper limits at 95% CL on the production cross section of a new resonance times its branching ratio to decay into a pair of vector bosons are derived as a function of the resonance mass. In fig. 3 the upper limits on $\sigma \times B(W' \to ZW)$ for the DY production of a $W'$ boson in the HVT model are reported as an example, combining $llqq$ and $\nu\nu qq$ searches, and on $\sigma \times B(G_{KK} \to WW + ZZ)$ for the DY production of a bulk RS graviton, in $qqqq$ search. The observed limits are compared with theoretical predictions of HVT models and RS graviton models leading to exclusion limits on the mass for the various signal hypotheses. In $llqq/\nu\nu qq$ searches, for HVT Model A (Model B) with coupling constant $g_V = 1$ ($g_V = 3$), a spin-1 vector triplet produced via the DY process is excluded for $m(W') < 2.9$ (3.2) TeV. In fully hadronic search, for the bulk RS model with $k/\overline{M}_{Pl} = 1$, a spin-2 Kaluza-Klein graviton is excluded in the range 1.3–1.8 TeV.

REFERENCES

[1] Evans L. and Bryant P., *JINST*, **3** (2008) S08001.
[2] Branco G. C. *et al.*, *Phys. Rep.*, **516** (2012) 1.
[3] Pappadopulo D., Thamm A., Torre R. and Wulzer A., *JHEP*, **09** (2014) 060.
[4] Randall L. and Sundrum R., *Phys. Rev. Lett.*, **83** (1999) 3370.
[5] Carvalho A., arXiv:1404.0102 [hep-ph].
[6] ATLAS Collaboration, *JINST*, **3** (2008) S08003.
[7] ATLAS Collaboration, *JHEP*, **09** (2019) 91.
[8] ATLAS Collaboration, *JHEP*, **03** (2018) 009.
[9] ATLAS Collaboration, *JHEP*, **03** (2018) 042.
[10] ATLAS Collaboration, *Eur. Phys. J. C*, **77** (2017) 317.
[11] Larkoski A. J., Moult I. and Neill D., *JHEP*, **05** (2016) 117.
[12] ATLAS Collaboration, *Improving jet substructure performance in ATLAS using Track-CaloClusters*, Tech. Rep. ATL-PHYS-PUB-2017-015 (CERN, Geneva) July 2017.
[13] Choudalakis G. and Casadei D., *Eur. Phys. J. Plus*, **2** (2012) 127.